

ORIGINAL RESEARCH ARTICLE

An improved fuzzy c-means-raindrop optimizer for brain magnetic resonance image segmentation

Bindu Puthentharayil Vikraman, Jabeena Afthab*

School of Electronics Engineering, Vellore Institute of Technology, Vellore 632014, India

* Corresponding author: Jabeena Afthab, bindu.pv2018@vitstudent.ac.in, ajabeena@vit.ac.in

ABSTRACT

The performance of healthcare systems, particularly regarding disease diagnosis and treatment planning, depends on the segmentation of medical images. Fuzzy c-means (FCM) is one of the most widely used clustering techniques for image segmentation due to its simplicity and effectiveness. FCM, on the other hand, has the disadvantages of being noise-sensitive, quickly settling on local optimal solutions, and being sensitive to initial values. This paper suggests a fuzzy c-means clustering improved with a nature-inspired raindrop optimizer for lesion extraction in brain magnetic resonance (MR) images to get around this constraint. In the preprocessing stage, the possible noises in a digital image, such as speckles, gaussian, etc., are eliminated by a hybrid filter—A combination of Gaussian, mean, and median filters. This paper presents a comparative analysis of FCM clustering and FCM-raindrop optimization (FCM-RO) approach. The algorithm performance is evaluated for images subjected to various possible noises that may affect an image during transmission and storage. The proposed FCM-RO approach is comparable to other methods now in use. The suggested system detects lesions with a partition coefficient of 0.9505 and a partition entropy of 0.0890. Brain MR images are analyzed using MATLAB software to find and extract malignancies. Image data retrieved from the public data source Kaggle are used to assess the system's performance.

Keywords: FCM; clustering; raindrop optimization; MR image; image segmentation

ARTICLE INFO

Received: 12 July 2023

Accepted: 24 July 2023

Available online: 5 September 2023

COPYRIGHT

Copyright © 2023 by author(s).

Journal of Autonomous Intelligence is published by Frontier Scientific Publishing.

This work is licensed under the Creative Commons Attribution-NonCommercial 4.0

International License (CC BY-NC 4.0).

<https://creativecommons.org/licenses/by-nc/4.0/>

1. Introduction

Image segmentation is a hotspot and focal point for image processing techniques. Segmenting an image into smaller sectors with remarkably homogeneous features enables extracting some critical data. It assembles portions of an image that have similar characteristics or properties. In segmentation, images are divided based on the pixels' color, directed gradient histograms, local binary patterns, etc.^[1]. Segmentation is helpful in many different domains, including remote sensing, geographic information systems, medical imaging, and many more^[2]. Medical imaging uses segmentation for various purposes, including image representation, feature extraction, and measurement. The identification of tumors, the classification of blood cells, the simulation of surgeries, the detection of coronary borders in angiograms, the detection of microcalcifications on mammograms, and other processes all depend on image segmentation^[3-6].

Different segmentation techniques are already in use in numerous applications. There are two categories of image segmentation methods: (1) A discontinuity-based technique, which relies on abrupt variations in pixel intensity values, and (2) a similarity-based strategy, which works based on the homogeneity requirement^[7-11]. A discontinuity-

based method identifies isolated points, edges, or lines, and a similarity-based technique groups pixels with similar intensities^[12]. The segmentation methods based on thresholding, region enlarging, region splitting, and merging are all included in the similarity strategy. In thresholding, pixels with intensity values over a predetermined threshold form a cluster. In the region-growing technique, we start with a set of seed points and pixels with the same intensity value to develop a specific bunch. The region-growing method expands regions based on proximity and similarity^[13-14]. The input image is separated into smaller images in the split and merge approach, and smaller sub-images with similar qualities are combined to create a more noticeable segment^[15-18].

The fundamental region-growing technique in fuzzy c-means (FCM) clustering divides pixels into appropriate segments according to their membership grades. FCM is a probability-based soft clustering algorithm^[19-21]. One data point in this algorithm might be a member of several clusters. FCM has emerged as one of the most popular clustering techniques due to its ease of use and potency. FCM, on the other hand, has the disadvantages of being noise sensitive, quickly sinking into local optimal solutions, and being keen on preliminary values^[22-23].

Optimized clustering of data in FCM algorithms uses metaheuristic optimization techniques. The raindrop optimization algorithm (ROA) is a metaheuristic algorithm enthused by how raindrops naturally fall down a valley when they descend a slope^[24-26]. After a few iterations, the population size falls, and larger droplets with a broader inquiry domain appear.

Zotin et al.^[27] proposed an image segmentation technique using FCM clustering. Before clustering, the image underwent preprocessing to eliminate any possible noise in the picture. The canny edge detection tool identifies the images' delicate borders. Mishro et al.^[28] introduced a type 2 FCM clustering technique for segmenting brain MR images. A fixed value for the fuzzifier and potential noise in the collected image has a substantial negative impact on the execution of an FCM clustering algorithm. An adaptive fuzzy linguistic fuzzifier value replaces the fixed fuzzifier in this approach. Including spatial features in the membership decreases the misclassification of the noisy pixels. An FCM clustering method for segmenting tumors from a brain MR image was presented by Mohammed and Al-ani^[3]. They cited different imaging modalities and FCM clustering procedures in their work.

The UNet++ architecture was presented by Zhou et al.^[29] for precise and practical image segmentation. They used a collection of U-nets with different depths that collaborated on learning while closely supervised. A versatile feature fusion technique was created by rebuilding skip connections at the decoder sub-networks to combine features of varying semantic sizes. Trimming accelerated the processing speed. Data from six medical imaging sensory systems, including computed tomography (CT), electron microscopy (EM), and others, were used to evaluate the system's performance. TransUNet, a technique for picture segmentation that combines transformers and U-net, was proposed by Chen et al.^[30]. Using a tokenized image patch as input, the transformer extracts global contexts from a convolution neural network (CNN) feature map. Before merging the encoded features with the resolution-enhanced CNN feature maps, the decoder up samples them for exact localization. The results show that the suggested technique performs better by recovering localized spatial information. The advantages and disadvantages of network architectures and image segmentation approaches were evaluated by Hesamian et al.^[31]. They thoroughly explained the problems deep learning-based segmentation algorithms encounter and possible solutions in their study. ResUNet++, an enhanced ResUNet design for segmenting colorectal polyps in colonoscopic images, was introduced by Jha et al.^[32]. The outcomes demonstrate that adding residual units, ASPP, and other elements enhanced the system's performance.

Dhanachandra and Chanu^[33] presented an FCM algorithm optimized with a dynamic particle swarm optimizer. This algorithm dynamically updated the learning parameters and inertia weight. A noise reduction method based on nearby pixels enhanced the anti-noise capacity. Moazzeni and Khamehchi^[26] demonstrated the rain optimization method (ROA), a metaheuristic optimization process triggered by precipitation. The

algorithm initialized the population size, raindrop radius, and other tuning parameters. The cost function gives each droplet a value. The droplets start to fall one by one at that point. The cost function would examine each droplet's endpoint to address this issue. A droplet will proceed along its course as it starts to move until it reaches the slightest obstruction. Each droplet would experience an identical process. The speed of the algorithm might increase if nearby droplets combine their paths. The droplet's radius gradually decreases as it approaches its lowest radius, significantly increasing the precision of the response. This method enables the algorithm to locate every target function extremum position. Kaboli et al.^[34] used the rain optimization approach as a practical remedy for multi-dimensional numerical test optimization functions. The proposed method was artless of the parameter selection and thus retained its usefulness for handling constrained optimization problems. They evaluated the algorithm's performance against other heuristic search techniques and discovered comparable outcomes. Mirjalili et al.^[24] presented GWO approaches that mimic grey wolves' social structure and stalking tactics in the wild. The performance of the proposed algorithm was comparable to that of the metaheuristic approaches like PSO, GSA, etc. Mohammadian-Khosnoud et al.^[25] presented a hybrid FCM-GWO algorithm to separate the nucleus of a cell from the other dark objects in it. The hybrid algorithm achieved better V_{pc} and V_{pe} indices than the FCM approach, while its performance was poor in Davies-Bouldin and Calinski-Harabasz indices.

Kirillov et al.^[35] presented a method for segmenting images using traditional computer graphics. They displayed a rendering network model based on neural networks. The execution of point-based segmentation projections at configurable chosen locations constitutes an iterative subdivision technique.

Table 1 shows a comparative analysis of algorithms used for optimization.

Table 1. Comparative analysis of optimization techniques.

Sl. No.	Optimization technique	Concept	Advantage	Disadvantage	Reference
1	Genetic algorithm (GA)	An evolutionary algorithm inspired by Charles Darwin's theory of evolution.	It works best in situations where a huge search space area has several factors in it.	Sensitive to initial conditions and may not reach the global optimum.	[36]
2	Particle swarm optimization (PSO)	Population-based stochastic optimization algorithm inspired by social behavior of bird flocking.	Fast computing speed and parallel processing.	In high-dimensional space, there is more probability of falling into a local optimum and a low convergence rate during the iterative process.	[37,38]
3	Gray wolf optimization (GWO)	Compared to PSO and GA, GWO has the advantages of fewer parameters, simple principles, and implementation quickly.	Slow convergence speed, low solution accuracy.	The chances of falling in local optimum are less.	[25,39]

A detailed analysis of current methods suggests that more accurate segmentation can improve lesion identification and diagnosis. So, to extract lesions from MR images, this paper presents the FCM clustering method supplemented with the RO algorithm.

The rest of the research paper's organization is as follows. section 2 describes the suggested approach, while section 3 discusses the implementation outcomes. Section 4 presents the central conclusion and then references.

2. Proposed methodology

Digital imaging is critical to medical research, diagnosis, and therapy planning. Image segmentation algorithms are frequently used in diagnosis, for instance, to assess anatomical features and to remove lesions^[30,31].

The three elements of a healthy brain are white matter, cerebrospinal fluid, and grey matter. Lesions in the brain can have a variety of characteristics. Medical image segmentation extracts lesions, the medically relevant parts called the region of interest (RoI), from the non-region of interest (NRoI) background information. This study uses feature-based clustering to identify lesions from brain MR images.

Figure 1 depicts the workflow model of the proposed system.

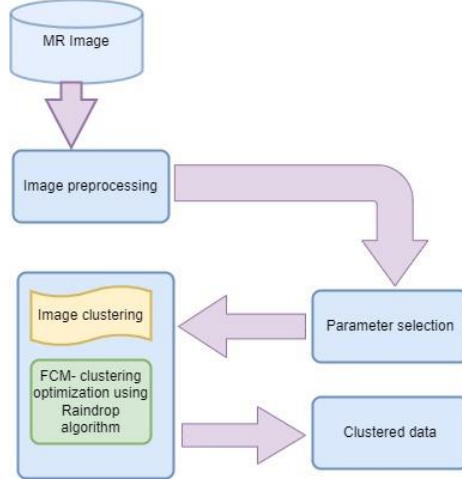


Figure 1. Workflow model of the proposed algorithm.

The dataset for the algorithm evaluation is from the public source Kaggle dataset. The image in the dataset has a resolution of 240×240 pixels. A hybrid filter is used in the preprocessing stage to eliminate the possible noise in the image. The proposed system applies a feature-based clustering approach. The cluster centroid selection is optimized using the raindrop algorithm.

2.1. Image pre-processing

Pre-processing is the process of improving the quality of an image. This pre-processing technique suppresses the undesired image distortions and improves the crucial image attributes required for future processing. Because of transmission and acquisition problems, medical images are particularly susceptible to noise. Moreover, MR images are more vulnerable to noise, such as salt and pepper noise, Gaussian, and speckle, which affects the quality of MR images. A hybrid filter—a combination of Gaussian, mean, and median filters is used in the preprocessing stage to denoise the image.

The Equations (1)–(3) provide the mathematical representation of these filters.

$$\text{Mean filter, } MF = \frac{1}{N} \sum_{p=-a}^a \sum_{q=-b}^b g[x, y] \quad (1)$$

where, N indicates the number of pixels considered, x and y denote the pixel location.

$$\text{Gaussian filter, } GF(p, q) = \frac{1}{2\pi\sigma^2} e^{-\frac{p^2+q^2}{2\sigma^2}} \quad (2)$$

where, σ depicts Gaussian distribution, and p, q indicates the rows and columns of the Gaussian function.

$$\text{Median filter} = \text{Med}\{Md_k\} \left\{ \begin{array}{ll} Md_k^{(n+1)/2}, & n \text{ is odd.} \\ 1/2 [Md_k^{(n/2)} + Md_k^{(n/2) + 1}], & n \text{ is even.} \end{array} \right\} \quad (3)$$

2.2. Raindrop optimized FCM clustering approach

Hard clustering and soft clustering are two different types of clustering techniques. In hard clustering, a single data point could only fit into a single group; however, it may belong to numerous groups in soft

clustering. FCM is a fuzzy clustering technique with a probability emphasis. A single data point may belong to many clusters when using this method^[29,40-42].

The dataset consists of n input data points, $P = \{p_1, p_2, p_3, \dots, p_n\}$ that can be grouped into C clusters, $C = \{C_1, C_2, C_3, \dots, C_C\}$. The FCM algorithm tries to reduce the objective function in Equation (4) by altering the membership function and cluster center degree in each iteration.

$$J = \sum_{i=1}^C \sum_{j=1}^n U_{ij}^m D_{ij}^2 \quad (4)$$

where, m is the fuzzification element, U_{ij} is the membership degree and D_{ij} the euclidean distance of j -th instance to i -th cluster centroid and is given by the Equation (5). Degree of membership of p_i in j -th cluster is given by the Equation (6) and the cluster centroid is given by the Equation (7).

$$D_{ij} = \|P_i - C_j\| \quad (5)$$

$$U_{ij} = \frac{D_{ij}^{\frac{2}{1-m}}}{\sum_{k=1}^C D_{kj}^{\frac{2}{1-m}}}, i \in [1, C], j \in [1, n] \quad (6)$$

$$C_i = \frac{\sum_{j=1}^n U_{ij}^m P_j}{\sum_{j=1}^n U_{ij}^m}, i \in [1, C] \quad (7)$$

The ROA is a metaheuristic algorithm stirred by how raindrops fall as they push from a mountainside to a valley^[43]. If a droplet falls on a level surface, it may be absorbed into the soil or evaporate. If it falls on an inclined surface, it may flow downward and congregate with other droplets to form a stream. Based on the soil characteristic and the earth's topography, individual droplets may form lakes that reflect local minima. By choosing a better outcome than a forecast based on the gradient of the objective function, RO simulates this bias. The situation will be different if the droplet size is large. Flooding can occur when large droplets quickly mix without evaporation or soil absorption. Parameter tweaking is essential in raindrop optimization. The initial population of the raindrop optimization algorithm was created randomly on the first iteration as a nod to the randomness of raindrop fall. Before the drop traveled toward the neighbor point with the lowest position, the drop's neighbor points' positions were compared with the drop itself. Until it reaches the valley, the raindrops will keep falling. Even if puddles are on the road to the valley, the RO algorithm generates a suitable mechanism to overspill and emerge from the puddles, allowing them to continue their journey to the canyon^[19,34]. The radius of a raindrop might be reduced by evaporation or absorption, but interactions with other raindrops may also increase it. Each droplet's radius is selected at random from a suitable range. Each droplet inspects its neighborhood iteratively, whose basis is its size. Find the last point in the region a droplet has covered if it doesn't connect to another droplet. While attempting to solve a problem in n dimensions, each droplet has n variables. As a result, the minimum and maximum limits are calculated first because the droplet's radius will determine these limits^[6,10]. The next step is testing the second variable's two endpoints until the last one evaluates. The first droplet's cost changes when it pushes lower, which is not the final move; instead, it will decrease the same way the cost function does. After repeating this process for all the droplets, each droplet's price and location are calculated. There are two ways to alter the radius of each droplet. This algorithm can locate global and local extremum if its parameters are adjusted correctly.

The algorithm's first iteration starts with the randomly generated initial population. Assume that s represents the population size. Therefore, Equation (8) defines the drop figure D^n .

$$D^n = [p_{n,1}, p_{n,2}, p_{n,3}, \dots, p_{n,m}], n \in \{1,2,3, \dots, s\} \quad (8)$$

where m is the optimization variables, p is the optimization problem variable and $P_{n,k}$ is the k -th variable of optimization task.

Rainfall properties are modeled as a uniform random distribution function bound by the constraint in Equation (9) throughout the optimization phase.

$$p_{n,k} = U(\text{low}_k, \text{upp}_k) \quad (9)$$

where $\text{low}_k, \text{upp}_k$ indicates the minimum and maximum bounds of p_k and U indicates the uniform distribution function.

A randomly generated point b about drops j , NP_j^b is represented as Equation (10).

$$\begin{aligned} \|(D^b - NP_j^b) \cdot \hat{u}_k\| &\leq \|r \cdot \hat{u}_k\| \\ b = \{1,2,3, \dots, s\}; k &= \{1,2,3, \dots, m\} \\ r &= r_{\text{initial}} \times f_{\text{iteration}} \end{aligned} \quad (10)$$

where r indicates the neighborhood size, r_{initial} the initial neighborhood size and $f_{\text{iteration}}$ indicates the step size within the iteration and \hat{u}_k indicates the unit vector of k -th dimension.

If G indicates the objective function, the dominant neighbor point NP_d^i satisfies the constraint given in Equations (11) and (12).

$$G(NP_d^i) < G(D^i) \quad (11)$$

$$G(NP_d^i) < G(NP_j^i), j \in \{1,2,3, \dots, np\} - \{d\} \quad (12)$$

when two droplets of radius r_1 and r_2 are near enough to share a common area, they can join to build a larger droplet of radius R given by the Equation (13). If a droplet of radius r_1 does not advance because of soil characteristics, the expression becomes Equation (14).

$$R = (r_1^m + r_2^m)^{1/m} \quad (13)$$

$$R = (\alpha r_1^m)^{1/m} \quad (14)$$

where, α indicates the volume percentage of droplet and varies between 0–100 percent in each iteration.

After a few iterations, the population size falls, and larger droplets with a broader inquiry domain appear. As a result, increasing the number of iterations speeds up the finding of reasonable solutions. As a result, the cluster group is produced in the shortest period while minimizing noise by increasing the overall number of iterations.

2.3. Proposed system flowchart

Figure 2 shows the flowchart of the proposed algorithm. The algorithm segments the brain MR image into RoI and non-RoI. So, the number of clusters is initialized as 2. Parameters of the RO algorithm, such as the population, raindrop position, neighborhood size, iteration step size, and objective function, are initialized. Randomly generated the initial fuzzy partition matrix and computed the membership function. Until it reaches the ideal objective function, each raindrop's position, velocity, and fitness function are calculated and updated. The output of the RO method is used to calculate the cluster centroid and objective function in the FCM algorithm. Two clusters are generated when the goal function comes to the minimum value. As a result, the cluster group (ROI and non-ROI) is formed with the least time and noise by increasing the total number of repetitions.

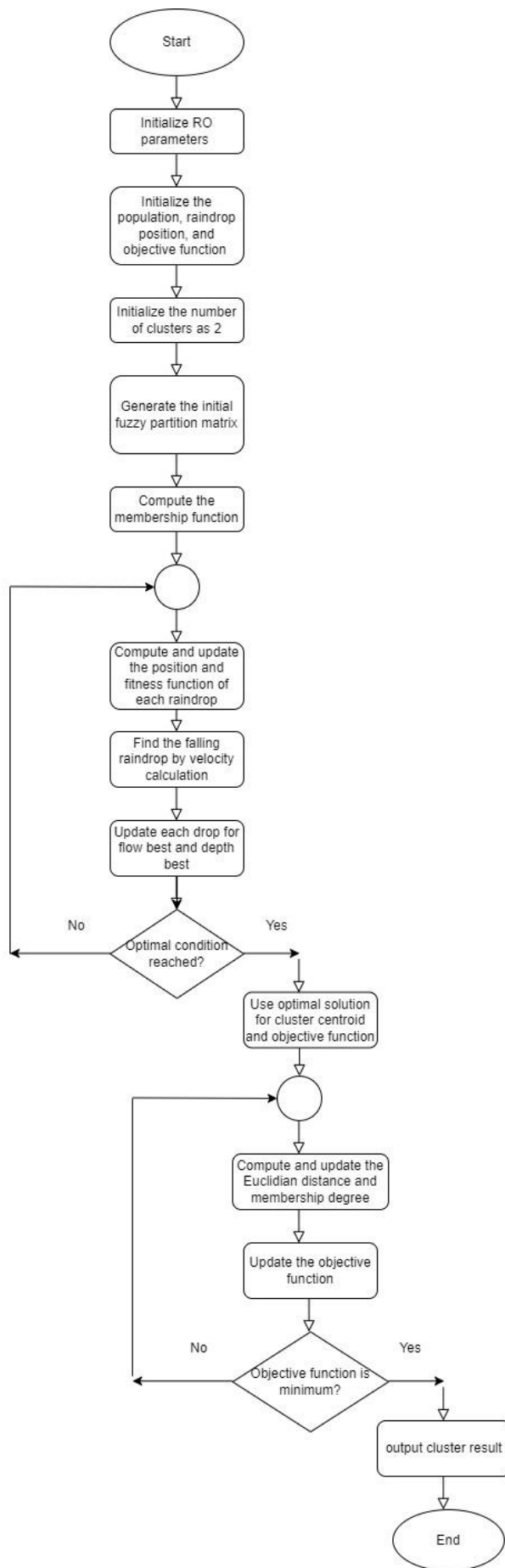


Figure 2. Proposed algorithm flowchart.

3. Results and discussions

This section looks at the experimental findings made possible by the suggested technique. MATLAB 2021a is used to carry out the proposed strategy.

3.1. Information on dataset

The public source Kaggle dataset^[44] is the basis for the algorithm evaluation. This dataset is a personal collection of brain tumor-specific T1, contrast-enhanced T1, and T2 magnetic resonance images. Without any tagging or patient identification, the images were gathered, reviewed by radiologists, and made available for research. The image data has a resolution of 240×240 pixels.

Figure 3 shows the images used in the algorithm evaluation.

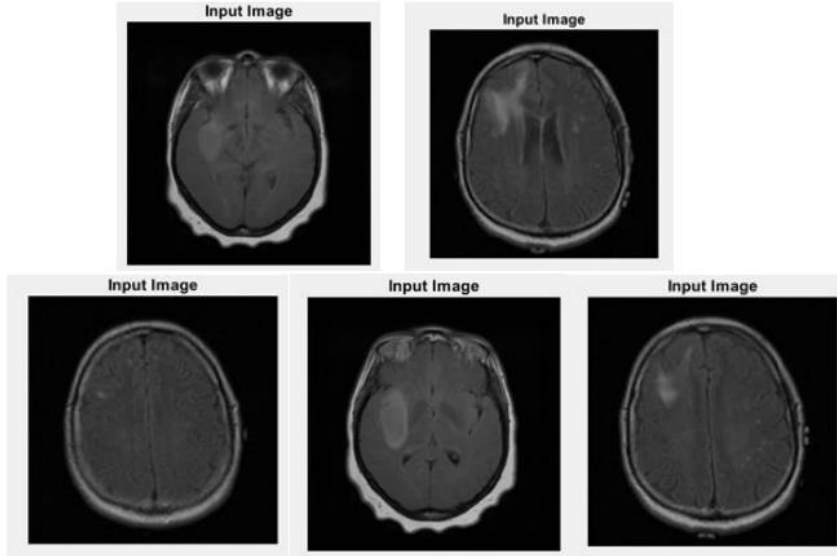


Figure 3. Images used for the lesion extraction.

3.2. Performance metrics

Partition coefficient PC and partition entropy PE , defined by Equations (15) and (16), are used as the evaluation metrics.

$$PC = \frac{\sum_i^N \sum_j^C U_{ij}^2}{N} \quad (15)$$

$$PE = \frac{\sum_i^N \sum_j^C U_{ij} \log U_{ij}}{N} \quad (16)$$

3.3. Algorithm performance analysis

This section demonstrates the outcomes derived from the proposed algorithm. **Figure 4** displays the obtained output at different stages of the FCM approach. The input image is of resolution 240×240 pixels. The FCM algorithm segments the input image into RoI and non-RoI. The PC value varies from 0.7819 to 0.8338 for five MR images, with an average value of 0.8086. The PE value ranges from 0.3256 to 0.4138, with an average value of 0.369 for the five selected images.

Figure 5 shows the output at various stages in the optimized RO-FCM approach. The proposed algorithm segments the input image into RoI and non-RoI. To accomplish ideal clustering, PC and PE must be in their

highest and lowest positions. In the $[0, 1]$ space are PC and PE . The PC value varies from 0.9429 to 0.9583 for five MR images, with an average of 0.9505. The PE value range from 0.0756 to 0.0999, with an average value of 0.0890 for the five selected images. Given that the mean PC value of the suggested algorithm is 0.9505, which is closer to one, and that the PE value is 0.0890, which is closer to zero, it performs comparable to existing algorithms.

Table 2 presents a performance comparison of PC and PE for the above five different MR images in the data set.

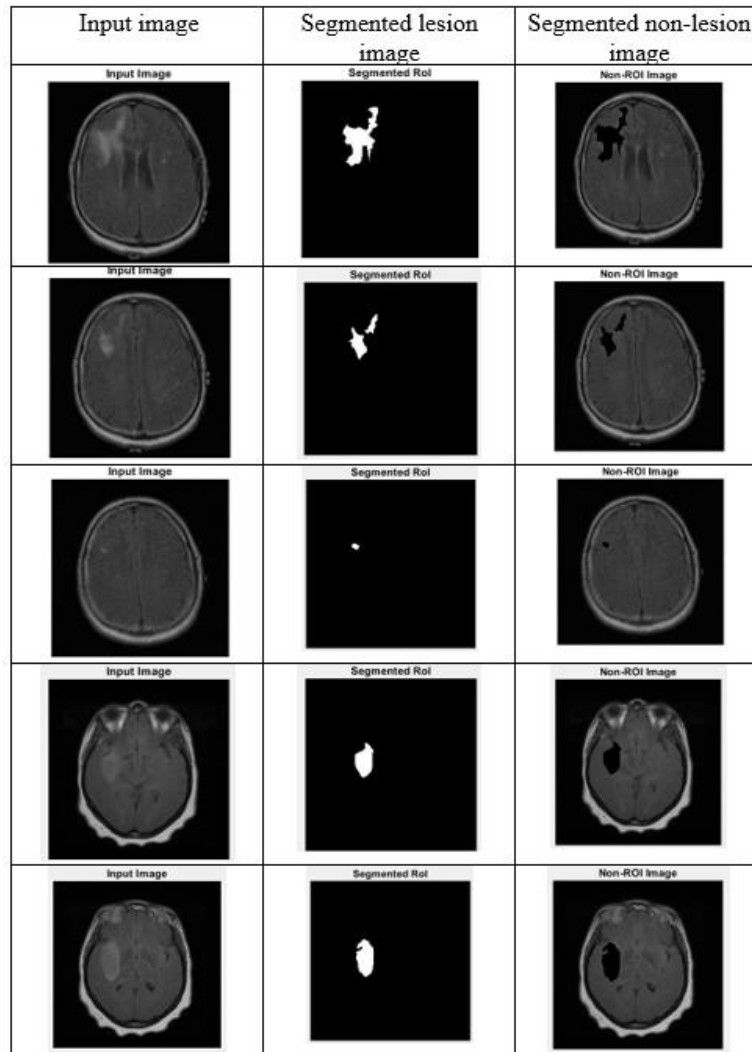


Figure 4. Segmentation outcomes of the FCM approach.

Table 2. Performance comparison in terms of PC and PE .

Sl. No.	FCM		RO-FCM		Time elapsed in seconds (RO-FCM)
	Partition coefficient (PC)	Partition entropy (PE)	Partition coefficient (PC)	Partition entropy (PE)	
1	0.7819	0.4138	0.9462	0.0978	0.805095
2	0.8191	0.3519	0.9429	0.0999	0.673290
3	0.8119	0.3629	0.9583	0.0756	0.684236
4	0.7962	0.3908	0.9499	0.0905	1.521729
5	0.8338	0.3256	0.9550	0.0813	1.549656
Mean	0.8086	0.369	0.9505	0.0890	1.046801

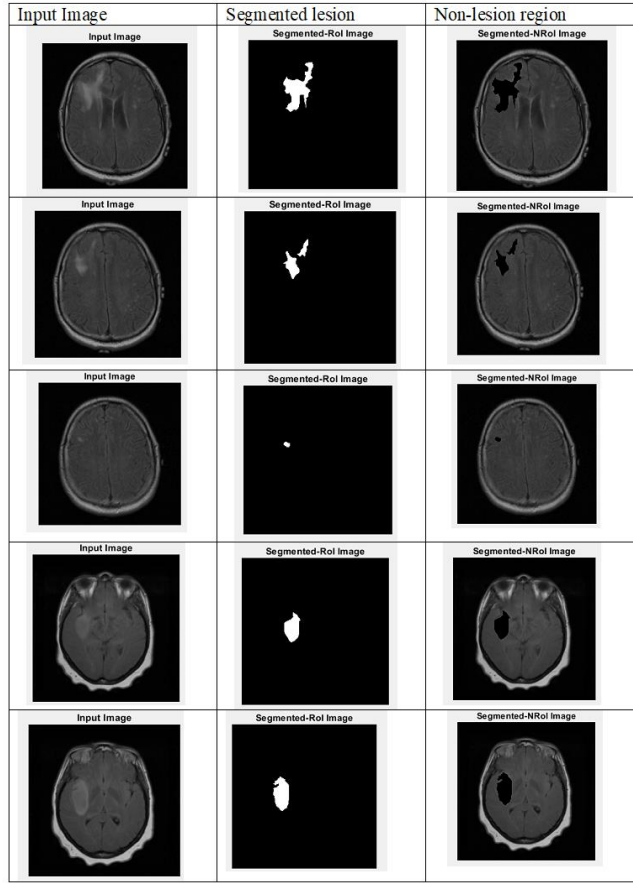


Figure 5. Segmentation outcomes of the RO-FCM approach.

Figure 6 shows the graphical illustration of the performance comparison.

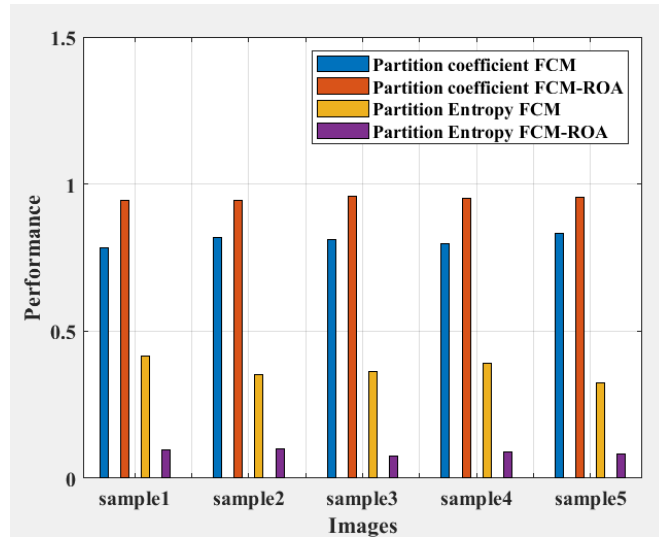


Figure 6. Performance comparison in terms of PC and PE .

Optimal clustering attains when PC and PE are at their highest and lowest points, respectively. The FCM technique yielded a mean PC value of 0.8086 and a PE of 0.3690. When compared to the FCM method, the RO-FCM algorithm performs better. The RO-FCM approach induces better clustering since its mean PC value is 0.9505, closer to one, and the PE value is 0.0890, more comparable to zero.

The noise in the image impacts how well the proposed algorithms perform. The most common type of image noise is additive white gaussian noise^[45]. Table 3 shows the performance indicator values for the RO-

FCM method for noise-affected and noise-filtered images. The performance is evaluated using images subjected to salt and pepper noise with a noise density of 0.02 and Gaussian noise with a mean of 0.01.

Figure 7 shows the graphical illustration of the performance comparison in **Table 3**. The algorithm's performance declines for the images with noise problems. Image preprocessing for eliminating noise takes place before segmentation. A sequence of mean-median filters performs the noise removal task. The average *PC* for the five noise-affected photos is 0.9061, less than the noise-free image, and the average *PE* is 0.1654, more than the noise-free image.

Table 4 compares the proposed approach to SFCM^[23], AWSFCM^[28], DPSO-FCM^[33], and E-based FCM^[46] in terms of *PC* and *PE* values.

Table 3. RO-FCM performance indicators for noise affected images.

Sl. No.	RO-FCM (Gaussian noise)		RO-FCM (salt & pepper noise)	
	Partition coefficient (<i>PC</i>)	Partition entropy (<i>PE</i>)	Partition coefficient (<i>PC</i>)	Partition entropy (<i>PE</i>)
1	0.8891	0.195	0.9361	0.1169
2	0.9182	0.1441	0.9544	0.0825
3	0.9052	0.1680	0.9483	0.0948
4	0.8963	0.1826	0.9391	0.1108
5	0.9219	0.1375	0.9486	0.0920
Mean	0.9061	0.1654	0.9453	0.0994

Table 4. Performance comparison with available approaches.

Technique	Partition coefficient (<i>PC</i>)	Partition entropy (<i>PE</i>)
SFCM	0.924	0.117
AWSFCM	0.9038	0.0475
DPSO-FCM	0.94	0.13
E-based FCM	0.921	0.106
FCM	0.8086	0.369
Proposed RO-FCM	0.9505	0.0890

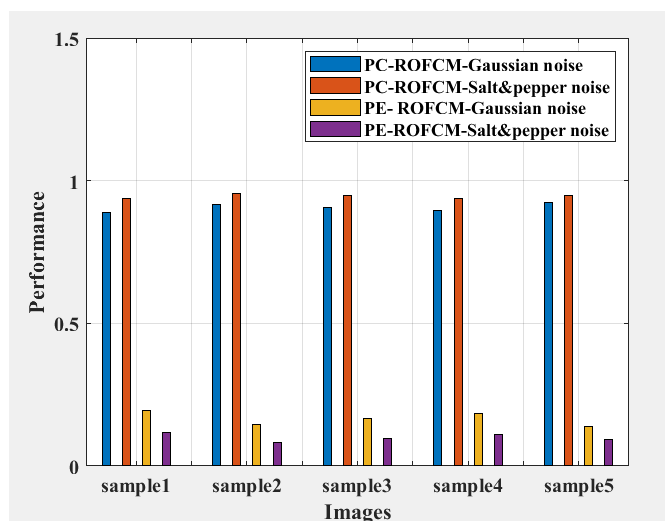


Figure 7. Performance comparison (noise affected image) in terms of *PC* and *PE*.

The RO-FCM performs significantly better than the alternative algorithms considered in the analysis. The RO-FCM algorithm has excellent *PC* and lower *PE* values than the FCM algorithm. FCM has a mean *PC* value of 0.8086 and a mean *PE* value of 0.3690 over five images, whereas RO-FCM has a mean *PC* value of 0.9505

and a mean PE value of 0.0890. The PC value of the RO-FCM is higher than the considered algorithms. The PE value of the RO-FCM approach is lower than the other approaches considered, except AWSFCM approach.

The average segmentation time for the five images considered in the proposed RO-FCM approach is 1.046801 s. The segmentation time in the KIFCM approach proposed by Abdel-Maksoud et al.^[47] is 12.87 s for 8 iterations. In the deep learning-attention mechanism approach proposed by Ranjbarzadeh et al.^[48], the segmentation time is 84 s and the on the U-net model approach of Lee et al.^[49] takes 4 h for the image segmentation. The performance metrics show that the proposed algorithm is a promising one in MR image segmentation.

4. Conclusion

This work presents efficient lesion extraction strategies for MR images utilizing the metaheuristic optimization technique, raindrop optimization, in fuzzy c-means clustering. The raindrop optimization algorithm addresses the quick settling on local optimal solutions and sensitivity to initial values problems of FCM clustering. A hybrid filter combines Gaussian, mean, and median filters in the preprocessing stage to eliminate any possible noise in the image. The dataset for the algorithm assessment is from the public Kaggle data source. This paper presents a comparative analysis of FCM clustering and FCM-raindrop optimization (FCM-RO) approach. The suggested RO-FCM method exhibits higher PC values than the FCM technique, and its PE value is lower than that of the FCM approach. FCM has a mean PC value of 0.8086 and a mean PE value of 0.3690 over five images, whereas RO-FCM has a mean PC value of 0.9505 and a mean PE value of 0.0890. The algorithm performance is evaluated for images subjected to various possible noises that may affect an image during transmission and storage. The proposed RO-FCM approach is comparable to other methods now in use. The suggested system detects lesions with a partition coefficient of 0.9505 and a partition entropy of 0.0890. By verifying the findings using more pertinent evaluation criteria and comparing them against equivalent algorithms already in use, we intend to extend the study in the future.

Author contributions

Conceptualization, BPV; methodology, BPV; software, BPV; validation, BPV; formal analysis, BPV; investigation, BPV; resources, BPV; data curation, BPV; writing—original draft preparation, BPV; writing—review and editing, BPV; visualization, BPV; supervision, JA; project administration, BPV. All authors have read and agreed to the published version of the manuscript.

Funding

This research received no external funding.

Conflict of interest

The authors declare no conflict of interest.

References

1. Sran PK, Gupta S, Singh S. Segmentation based image compression of brain magnetic resonance images using visual saliency. *Biomedical Signal Processing and Control* 2020; 62: 102089. doi: 10.1016/j.bspc.2020.102089
2. Norouzi A, Rahim MSM, Altameem A, et al. Medical image segmentation methods, algorithms, and applications. *IETE Technical Review* 2014; 31(3): 199–213. doi: 10.1080/02564602.2014.906861
3. Mohammed BA, Al-ani MS. Digital medical image segmentation using fuzzy c-means clustering. *UHD Journal of Science and Technology* 2020; 4(1): 51–58. doi: 10.21928/uhdjst.v4n1y2020.pp51-58
4. Christ MCJ, Parvathi RMS. Fuzzy c-means algorithm for medical image segmentation. In: Proceedings of the 2011 3rd International Conference on Electronics Computer Technology; 8–10 April 2011; Kanyakumari, India. pp. 33–36.

5. Habib RU. Optimal compression of medical images. *International Journal of Advanced Computer Science and Applications(IJACSA)* 2019; 10(4): 133–140. doi: 10.14569/IJACSA.2019.0100415
6. Kasute SD, Kolhekar M. ROI based medical image compression. *International Journal of Scientific Research in Network Security and Communication* 2017; 5(1): 6–11.
7. Guerrero-valadez JM, Martínez-rios F. Rain-fall optimization algorithm with new parallel implementations. *EAI Endorsed Transactions on Energy Web* 2020; 7(29): 1–13. doi: 10.4108/eai.13-7-2018.163981
8. Bindu PV, Jabeena A. Medical image compression: A leap on recent progress and publications. In: Komanapalli VLN, Sivakumaran N, Hampannavar S (editors). *Advances in Automation, Signal Processing, Instrumentation, and Control*. Springer, Singapore; 2021. Volume 700. pp. 2281–2289.
9. Sreenivasulu P, Varadarajan S. An efficient lossless ROI image compression using wavelet-based modified region growing algorithm. *Journal of Intelligent Systems* 2018; 29(1): 1063–1078. doi: 10.1515/jisys-2018-0180
10. Parikh SS, Ruiz D, Kalva H, et al. High bit-depth medical image compression with HEVC. *IEEE Journal of Biomedical and Health Informatics* 2018; 22(2): 552–560. doi: 10.1109/JBHI.2017.2660482
11. Chen YY. Medical image compression using DCT-based subband decomposition and modified SPIHT data organization. *International Journal of Medical Informatics* 2007; 76(10): 717–725. doi: 10.1016/j.ijmedinf.2006.07.002
12. UmaMaheswari S, SrinivasaRaghavan V. Lossless medical image compression algorithm using tetrolet transformation. *Journal of Ambient Intelligence and Humanized Computing* 2021; 12(3): 4127–4135. doi: 10.1007/s12652-020-01792-8
13. Singh M, Kumar S, Chouhan SS, Shrivastava M. Various image compression techniques: Lossy and lossless. *International Journal of Computer Applications* 2016; 142(6): 23–26. doi: 10.5120/ijca2016909829
14. Gonzalez RC, Woods RE. *Digital Image Processing*, 4th ed. Pearson Education; 2018.
15. Ramesh KKD, Kumar GK, Swapna K, et al. A review of medical image segmentation algorithms. Available online: <https://publications.eai.eu/index.php/phat/article/view/1211> (accessed on 31 August 2023).
16. Matheen MA, Sundar S. Histogram and entropy oriented image coding for clustered wireless multimedia sensor networks (WMSNS). *Multimedia Tools and Applications* 2022; 81(27): 38253–38276. doi: 10.1007/s11042-022-13060-2
17. Minaee S, Boykov Y, Porikli F, et al. Image segmentation using deep learning: A survey. *IEEE Transactions on Pattern Analysis and Machine Intelligence* 2022; 44(7): 3523–3542. doi: 10.1109/TPAMI.2021.3059968
18. Saritha S, Prabha NA. A comprehensive review: Segmentation of MRI images—Brain tumor. *International Journal of Imaging Systems and Technology* 2016; 26(4): 295–304. doi: 10.1002/ima.22201
19. Pustokhina IV, Pustokhin DA, Nguyen PT, et al. Multi-objective rain optimization algorithm with WELM model for customer churn prediction in telecommunication sector. *Complex Intelligent Systems* 2021; 9: 3473–3485. doi: 10.1007/s40747-021-00353-6
20. Matheen MA, Sundar S. A novel technique to mitigate the data redundancy and to improvise network lifetime using fuzzy criminal search Ebola optimization for WMSN. *Sensors* 2023; 23(4): 2218. doi: 10.3390/s23042218
21. Szilagy L, Benyo Z, Szilagy SM, Adam HS. MR brain image segmentation using an enhanced fuzzy c-means algorithm. In: Proceedings of the 25th Annual International Conference of the IEEE Engineering in Medicine and Biology Society; 17–21 September 2003; Cancun, Mexico. pp. 724–726.
22. Horváth J. Image segmentation using fuzzy c-means. Available online: <http://conf.uni-obuda.hu/sami2006/JurajHorvath.pdf> (accessed on 31 August 2023).
23. Chuang K, Tzeng H, Chen S, et al. Fuzzy c-means clustering with spatial information for image segmentation. *Computerized Medical Imaging and Graphics* 2006; 30(1): 9–15. doi: 10.1016/j.compmedimag.2005.10.001
24. Mirjalili S, Mirjalili SM, Lewis A. Grey wolf optimizer. *Advances in Engineering Software* 2014; 69: 46–61. doi: 10.1016/j.advengsoft.2013.12.007
25. Mohammadian-Khoshnoud M, Soltanian AR, Dehghan A, Farhadian M. Optimization of fuzzy c-means (FCM) clustering in cytology image segmentation using the gray wolf algorithm. *BMC Molecular and Cell Biology* 2022; 23(1): 9. doi: 10.1186/s12860-022-00408-7
26. Moazzeni AR, Khamsehchi E. Rain optimization algorithm (ROA): A new metaheuristic method for drilling optimization solutions. *Journal of Petroleum Science and Engineering* 2020; 195: 107512. doi: 10.1016/j.petrol.2020.107512
27. Zotin AG, Simonov K, Kurako M, et al. Edge detection in MRI brain tumor images based on fuzzy c-means clustering. *Procedia Computer Science* 2018; 126: 1261–1270. doi: 10.1016/j.procs.2018.08.069
28. Mishro PK, Agrawal S, Panda R, Abraham A. A novel type-2 fuzzy c-means clustering for brain MR image segmentation. *IEEE Transactions on Cybernetics* 2020; 51(8): 3901–3912. doi: 10.1109/TCYB.2020.2994235
29. Zhou Z, Siddiquee MR, Tajbakhsh N, Liang J. UNet++ : Redesigning skip connections to exploit multiscale features in image segmentation. *IEEE Transactions Medical Imaging* 2020; 39(6): 1856–1867. doi: 10.1109/TMI.2019.2959609
30. Chen J, Lu Y, Yu Q, et al. TransUNet : Transformers make strong encoders for medical image segmentation. *Computer Science* 2011; 1–13.

31. Hesamian MH, Jia W, He X, Kennedy P. Deep learning techniques for medical image segmentation: Achievements and challenges. *Journal of Digital Imaging* 2019; 32(4): 582–596. doi: 10.1007/s10278-019-00227-x
32. Jha D, Smedsrud PH, Riegler MA, et al. ResUNet++: An advanced architecture for medical image segmentation. In: Proceedings of the 2019 IEEE International Symposium on Multimedia (ISM); 9–11 December 2019; San Diego, USA. pp. 225–230.
33. Dhanachandra N, Chanu YJ. An image segmentation approach based on fuzzy c-means and dynamic particle swarm optimization algorithm. *Multimedia Tools and Applications* 2020; 79: 18839–18858. doi: 10.1007/s11042-020-08699-8
34. Kaboli SHA, Selvaraj J, Rahim NA. Rain-fall optimization algorithm: A population-based algorithm for solving constrained optimization problems. *Journal of Computational Science* 2017; 19: 31–42. doi: 10.1016/j.jocs.2016.12.010
35. Kirillov A, Wu Y, He K, Girshick R. PointRend : Image segmentation as rendering. In: Proceedings of the 2020 IEEE/CVF Conference on Computer Vision and Pattern Recognition (CVPR); 13–19 June 2020; Seattle, USA. pp. 9799–9808.
36. Lambora A, Gupta K, Chopra K. Genetic algorithm—A literature review. In: Proceedings of the 2019 International Conference on Machine Learning, Big Data, Cloud and Parallel Computing (COMITCon); 14–16 February 2019; Faridabad, India. pp. 380–384.
37. Li M, Du W, Nian F. An adaptive particle swarm optimization algorithm based on directed weighted complex network. *Sensor/Actuator Networks and Networked Control Systems* 2014; 2014(2): 1–7. doi: 10.1155/2014/434972
38. Rahman I, Vasant PM, Singh BSM, Abdullah-Al-Wadud M. On the performance of accelerated particle swarm optimization for charging plug-in hybrid electric vehicles. *Alexandria Engineering Journal* 2016; 55(1): 419–426. doi: 10.1016/j.aej.2015.11.002
39. Hou Y, Gao H, Wang Z, Du C. Improved grey wolf optimization algorithm and application. *Sensors* 2022; 22(10): 3810. doi: 10.3390/s22103810
40. Matheen MA, Sundar S. IoT multimedia sensors for energy efficiency and security: A review of QoS aware and methods in wireless multimedia sensor networks. *International Journal of Wireless Information Networks* 2022; 29: 407–418. doi: 10.1007/s10776-022-00567-6
41. Zhou H, Schaefer G, Shi C. Fuzzy c-means techniques for medical image Segmentation. In: *Fuzzy Systems in Bioinformatics and Computational Biology*. Springer; 2009. pp. 257–271.
42. Almahfud MA, Setyawan R, Sari CA, Setiadi DRAM. An effective MRI brain image segmentation using joint clustering (k-means and fuzzy c-means). In: Proceedings of the 2018 International Seminar on Research of Information Technology and Intelligent Systems (ISRITI); 21–22 November 2018; Yogyakarta, Indonesia. pp. 11–16.
43. Bindu PV, Afthab J. Region of Interest based medical image compression using DCT and capsule autoencoder for telemedicine applications. In: Proceedings of the 2021 Fourth International Conference on Electrical, Computer and Communication Technologies (ICECCT); 15–17 September 2021; Erode, India. pp. 1–7.
44. Feltrin F. Brain tumor MRI images 44 classes. Available online: <https://www.Kaggle.Com/Datasets/Fernando2rad/Brain-Tumor-Mri-Images-44c> (accessed on 31 August 2023).
45. Goyal B, Dogra A, Agrawal S, Sohi BS. Noise issues prevailing in various types of medical images. *Biomedical and Pharmacology Journal* 2018; 11(3): 1227–1237. doi: 10.13005/bpj/1484
46. Kahali S, Sing JK, Saha PK. A new entropy-based approach for fuzzy c-means clustering and its application to brain MR image segmentation. *Soft Computing* 2019; 23: 10407–10414. doi: 10.1007/s00500-018-3594-y
47. Abdel-Maksoud E, Elmogy M, Al-Awadi R. Brain tumor segmentation based on a hybrid clustering technique. *Egyptian Informatics Journal* 2015; 16(1): 71–81. doi: 10.1016/j.eij.2015.01.003
48. Ranjbarzadeh R, Kasgari AB, Ghouschi SJ, et al. Brain tumor segmentation based on deep learning and an attention mechanism using MRI multi-modalities brain images. *Scientific Reports* 2021; 11(1): 10930. doi: 10.1038/s41598-021-90428-8
49. Lee B, Yamanakkanavar N, Choi JY. Automatic segmentation of brain MRI using a novel patch-wise U-net deep architecture. *PLoS One* 2020; 15(8): e0236493. doi: 10.1371/journal.pone.0236493